Colloids and Surfaces A: Physicochemical and Engineering Aspects 632 (2022) 127808

Contents lists available at ScienceDirect

Colloids and Surfaces A: Physicochemical and Engineering Aspects

journal homepage: www.elsevier.com/locate/colsurfa

Thin film breakage in oil–in–water emulsions, a multidisciplinary study

Ola Aarøen [a,*], Enrico Riccardi [b,*], Titus S. van Erp [c], Marit Sletmoen [a]

[a] Department of Biotechnology and Food Science, Norwegian University of Science and Technology, Høgskoleringen 5, 7491 Trondheim, Norway
[b] Department of Informatics, UiO, Gaustadalléen 23B, 0373 Oslo, Norway
[c] Department of Chemistry, Norwegian University of Science and Technology, Høgskoleringen 5, 7491 Trondheim, Norway

GRAPHICAL ABSTRACT

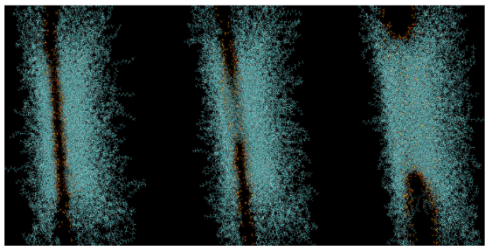

ARTICLE INFO

Keywords:
Optical tweezers
Emulsion
Surfactant
Coalescence
MD simulation
Thin film

ABSTRACT

Coalescence is a critical phenomenon in separation and transport processes. An improved understanding of coalescence can enhance current models predicting emulsion stability and separation. We here report a combined experimental and simulation study to investigate the thin film prior to its rupture in a coalescence event. Optical tweezers measured the influence of ions and of surface-active agents on coalescence time and the forces acting between colliding oil droplets. Molecular simulation described the composition and constituent distribution of the thin films in systems comparable with the ones investigated via optical tweezers. We identify a potential relationship between the disruption of the electrical double layer and the formation of nanocrystals with the thin film breakage times and depletion forces.

1. Introduction

Coalescence is controlled by the drainage and eventual rupture of the thin liquid film that develops between approached droplets [1]. Thin film drainage times and film rupture mechanism are strongly dependent on the forces between the molecules present at the interfaces. surface-active molecules can, therefore, significantly influence the processes. When amphiphilic molecules are present, they tend to form layers that cover the surface of the droplets [1–3]. Moreover, the solvent molecules interacting with the surfactants determine the behavior of the thin film formed between the two inter-phase regions. Solvent rearrangement and fluctuations in local surfactant density are effects that have been long neglected in the current emulsion models [4] with consequential limitation in the predictability of emulsion behaviors. In particular, emulsions comprised of crude oil and brine (petroemulsions) are significantly affected by the dynamics of coalescence between droplets, regarding their performance of transport and separation processes [1–3].

During the past decade, extensive experimental studies have been undertaken to characterize the rheological, thermodynamic, and

* Corresponding authors.
E-mail addresses: ola.aaroen@ntnu.no (O. Aarøen), enricori@ifi.uio.no (E. Riccardi).

https://doi.org/10.1016/j.colsurfa.2021.127808
Received 18 August 2021; Received in revised form 13 October 2021; Accepted 24 October 2021
Available online 27 October 2021
0927-7757/© 2021 The Authors. Published by Elsevier B.V. This is an open access article under the CC BY license (http://creativecommons.org/licenses/by/4.0/).

structural properties of interfacial layers composed of resin and asphaltene surfactants. The focus has mainly been posed on model oils employing model resin and asphaltene surfactants to facilitate well-controlled studies [5] as well as on real crude oils containing a myriad of indigenous resin and asphaltene surfactants in practical studies [2]. Molecular Dynamics simulations (MD) have provided further insight into the system. Riccardi and co-workers [5,6] recently found that the interface region behaves as a third phase in between the two adjacent bulk phases, and its properties are different from what could be predicted based on the knowledge of its composition and a simple linear component averaging. Dedicated investigations are therefore required to determine its behavior. As an example, it has been confirmed both theoretically and experimentally [7] that emulsions containing asphaltene type surfactants are effectively stabilized against coalescence when the interfacial concentration of the asphaltene approaches and exceeds 80% of its maximum attainable interfacial concentration. Other studies have reported that the inter-phase region in between two droplets formed by asphaltene and resin type surfactants give rise to a positive disjoining pressure [1,7–9].

Despite the experimental evidence [2] described above, current theoretical models for film drainage utilize relatively simple descriptions of surfactant behavior: London dispersion forces in oil continuous emulsions and through Derjaguin, Landau, Verwey, and Overbeek (DLVO) theory for water continuous emulsions [1,8]. In addition to the electrostatic and van der Waals forces in DLVO theory, the force of depletion arising from osmotic pressure due to concentration difference between bulk and thin film [10] will also affect the droplet collision behavior. Furthermore, limitations on available experimental techniques to either control or measure the distance separating the interphase regions of two approaching droplets, as well as the forces acting between the droplets, have hampered a reliable validation of film drainage models for coalescence [1,8]. Due to the complexity of the systems, it has not been possible to determine the relation(s) between the macroscopic behavior and the molecular mechanisms. Recent investigations have shown at a molecular level the importance of describing the structural and conformational rearrangements in the thin film generated between two droplets [9]. The interphase region is very sensitive to system modification in each neighboring phase and the induced structural modification must be described and accounted for. The description of the structural rearrangements occurring in the inter-phase region as a response to changes in various parameters (surfactant concentration and type, ionic strength, and type) requires molecular resolution [11]. The current continuous resolution models often fail to predict overall system behavior because they adopt a too superficial description of the disjoining pressure and film rupture mechanics. For petroemulsions in particular, the considered state-of-the-art models for film drainage during coalescence [1,8], are not in accordance with the stability mechanisms suggested by experimental studies [2].

Optical tweezers applied to emulsions have the potential to significantly reduce the previously mentioned experimental limitations. Ashkin was the first to demonstrate optical manipulation of micron-sized objects in laboratory experiments [12]. These famous experiments revealed that the radiation pressure of a beam of light could impart momentum on particles and push them along the path of light propagation. Later he showed how a small particle could be trapped in a small spacial volume by introducing a counteracting gradient force to the radiation pressure [13]. The gradient force is due to the Lorenz force and draws the particle toward the area of highest light intensity, i.e. toward the beam axis in case of a Gaussian beam profile, and toward the focus of the laser if the beam is focused. These discoveries lead to the “single--beam gradient force optical trap" [13], also referred to as an optical trap, or optical tweezers (OT), because of its ability to pick up and hold microscale particles. An optical trap is created by directing a laser beam with a Gaussian intensity profile through a lens of high NA, giving a tightly focused beam. A dielectric particle near the focus will experience a force due to the transfer of momentum from the scattering of the high number of incident photons. The resulting optical force has traditionally been decomposed into two components: a scattering force acting in the direction of light propagation and a gradient force acting in the direction of the higher light intensities along the intensity gradient. The gradient force is proportional to both the polarizability of the dielectric particle and the intensity gradient across the laser beam. For stable trapping in all three dimensions, the gradient force must be sufficient to balance the scattering force, and this is achieved in situations of a steep intensity gradient across the cross-section of the laser beam, produced by sharply focusing the trapping laser beam using the high numerical aperture objective lens.

The forces acting on a trapped particle can be described as a harmonic oscillator [14], where the particle is relatively firmly held, with the freedom to diffuse by Brownian motion [15]. The spring constant of the trap is obtained from a study of the restrictions induced by the optical trap on the Brownian motion [16]. By observing the outgoing beam profile using a QPD (quadrant photodiode) [17], any changes in the position of the trapped particle compared to the center of the optical trap, can be multiplied with the known spring constant of the trap. This (combined with accurate software-controlled optics) gives the OT set-up the ability to position particles with high precision while simultaneously measuring any 3D displacements of said particle with sub-micrometer and sub-millisecond accuracy and resolution, and also exert and quantify forces up to and beyond 10^{-10} N on particles ranging in size from nanometers to micrometer.

Since its invention, OT has been used in a wide range of research fields – from physics [18,19], to biology and medicine [20–22]. Several studies have also included a proof-of-concept for the applicability of OT in the field of emulsion research. These have focused on, among other things, emulsion droplets with ultralow interfacial tension, droplet deformation [23,24] and the formation of nanofluidic networks interconnecting droplets [25], pH dependant interactions between individual emulsion droplets [26], as well as the forces acting on droplets of micro and macromolecular stabilization [27]. Chen and coworkers have contributed with several advancements, including the quantification of interaction forces as functions of varying NaCl and sodium dodecyl sulfate (SDS) concentrations [28], later with non-ionic surfactant coating [29], and a switchable surface-active colloids system [30]. Otazo and coworkers have used OT for the study of coalescence. More precisely, they performed a study of partially crystalline emulsion droplets, with the aim to determine their propensity to aggregate or coalesce after being brought into contact [31]. Mitsunobo and coworkers studied temperature-induced coalescence on trapped emulsion droplets. [32] The coalescence of aerosol particles has been explored thoroughly in a single-beam optical trap [33], and using a holographic optical tweezer set-up [34,35]. Several previous papers focus on the use of optical tweezers to study depletion forces between colloidal particles [27–29,36]. Initial interactions between approaching interfaces will influence the probability of a coalescence event occurring, as they can increase the contact time between emulsion droplets in bulk. Previous work has also shown the effects of approach velocity on depletion forces and coalescence times in pristine oil-in-water emulsions [37]. In this work, we used OT to quantify the effect of ionic strength and surfactant density on the depletion force as well as the droplet coalescence times.

To interpret our experimental results, we complemented our study with atomistic computer simulations. The coalescence between two droplets requires the thinning and breakage of the thin film formed in between. While an actual coalescence event (the breaking of the thin film) is relatively quick, the steps leading up to the establishment of the thin film from initial contact and up to film breakage may take several seconds, even for unstabilized droplets [37]. Simulating coalescence at an atomistic scale would require unreachable amounts of computational resources. Dedicated strategies, therefore, need to be implemented. We adopted a step-wise approach to mimic the thin film thinning and breakage events. The approach provides also a necessary set-up to perform simulations with a more elaborated but demanding simulation

set-up as rare events [38–41]. These methods permit the investigation of events that are extremely unlikely but require knowledge of the transition under investigation and its potential energy landscape [42–44].

In the present work, we examine the thin film breakage in petroemulsions by the use of both optical tweezers based determination of depletion forces and coalescence times as well as molecular dynamics simulations aiming at determining the properties and thickness of the thin film prior to rupture.

2. Materials and methods

2.1. Preparation of emulsions and liquid cells

Emulsions were made by mixing dodecane oil, $C_{12}H_{26}$, (Sigma-Aldrich, St. Louis, USA) and de-ionized water (Milli-Q, > 18 MΩ cm^{-1}, Millipore). Additionally, NaCl (Sigma-Aldrich, St. Louis, USA) and the surfactant SDS (Sigma-Aldrich, St. Louis, USA) were added to the emulsions prior to mixing, bringing the final concentrations of 5, 20, and 100 mM NaCl, and 0.3, 3, 30 and 300 μM SDS. O/W emulsions of various stability were made by adding all components of the sample to an Eppendorf tube and performing a simple homogenization by vigorously shaking the sample tube on a vortex mixer (Fisher Scientific, Pittsburg, US) at 2000 rpm for at least 3 min. O/W emulsions were prepared in specific oil–to–water ratios in order to obtain suitable droplet density for trapping in the sample chamber. The droplet density in the sample cell must be sufficiently low to reduce the risk of trapping more than one droplet to an acceptable level, and sufficiently high to provide a sufficient density of droplets to trap. Based on an evaluation of the current method of emulsification and the desired size range of the oil droplets, a 1:10 ratio of oil to total sample volume was chosen. Immediately post homogenization, small volumes of emulsion were transferred to pre-prepared OT fluid cells and mounted in the microscope set up of the optical tweezers. The fluid cells used for the OT experiments were made by attaching a circular Borax glass (35 mm, thickness no. 1, VWR, Pennsylvania, US) to a rectangular cover glass (22×50mm, thickness no. 1, VWR, Pennsylvania, US) with two thin layers of double-sided tape, spaced roughly 0.5 – 1.0 cm apart. The height of the cell, therefore, equals the height of the two layers of tape and was in the range 100–200 μm, resulting in an internal volume of 20–30 μL.

2.2. Determination of depletion force and coalescence times using OT

The NanoTracker™ 2 optical tweezer instrument (JPK Instruments, Berlin, Germany) was used for the optical manipulation of the oil droplets. The instrument is mounted on a Zeiss Axio Observer Inverted optical microscope. It is equipped with a TEM00 laser, with a maximum power of 3 W. Each laser beam has a Gaussian profile, and they can be controlled independently of each other. A quadrant photodiode detector (QPD) located at the back-focal plane of the condenser objective detects any 3D displacement of the trapped objects relative to the laser focal point. Prior to measurements, two droplets that were observed to have a size within the chosen size range were trapped, one in each laser trap. The trap stiffness was determined for each trap based on the power spectrum, which was obtained by tracking the random 3D Brownian motion of the trapped droplets.

Droplets of a size that fell within the pre-specified size range were trapped and moved away from the glass surface to avoid sticking to the surface during and prior to the experiments. As the OT instrument allows for precise position control of the optical traps, the experiments aiming at determining depletion forces were performed by moving one of the traps towards the other until the droplets came in contact. Droplet point of contact was observable as an increase in tweezers force output, in the range of pico-Newtons. Although the force applied from the tweezers now press the droplet interfaces towards each other, it is not sufficient for any droplet deformation, which would require an ultra-low interfacial tension of the droplets [24]. Droplets were maintained in contact for 0.5 s before moving the traps back to their initial positions, where they were kept for 0.5 s to remove drift due to drag force. An illustration of trapped droplets approaching (retracting), and extending can be seen in Fig. 1 (*top left* and *top right*, respectively). Fig. 1*Bottom left* shows the recorded force output of both segments, and *Bottom right* the difference, the depletion curve. These steps were repeated until 20 force-displacement curves were recorded. Recorded force-displacement curves were plotted and processed using a Savitzky-Golay filter (bins:200, order:3), and the smoothed retract curve was subtracted from the extend curve to obtain the difference in forces acting on droplets during extend segments as compared to retract segments. This procedure is expected to result in flat curves containing a positive peak due to the attractive force acting between the oil droplets when separating them after first having brought them in contact. The height of this peak reflects the depletion force necessary to separate droplets.

For the determination of coalescence times, the optical traps were subjected to a different movement scheme. Instead of stopping the approach at droplet contact, traps were approached to the full overlap of focal points, ensuring full contact of droplets and emulating collisions occurring during droplet sedimentation. Droplets were left in contact and the time duration from reaching the contact point until coalescence occurred, was determined. The droplets were left in contact for up to a maximum of 6 min, a limitation of the system resources of the computer controlling the instrument. If no coalescence was observed during this time the experiment was considered a failure. For each sample composition, the coalescence time was determined for three independent droplet pairs and the results were averaged.

During both schemes, the approach velocity was fixed at 10 μm/s, as it is an important factor influencing both the depletion force and the coalescence time. The choice of concentration range for both NaCl and SDS was based on our previous observations on coalescence in optical traps [37]. The concentration range chosen covered the range within which coalescence is expected to occur. It also extended into the range where coalescence is not expected, due to too high concentrations of surfactant as well as an insufficient ionic strength of the bulk compared to the expected requirements for thin film formation and subsequent breakage.

2.3. MD simulation of the rupture process of thin films

The interphase layer between two approaching dodecane droplets was studied via full atom molecular dynamics simulations. This layer is composed of water, ions, and surfactants. The ions considered in the current study are Na^+ and Cl^-, while the surfactant is SDS. The ions and the dodecane molecules were simulated according to the OPLS-AA force field [45], water molecules with the TIP4p/2005 model [46], while SDS was simulated with an improved version of OPLS-AA for the surfactant [47]. A set of 36 simulations at different SDS and ion concentrations were performed. For a water/oil surface area of 16×16 nm^2, 8, 32, 72, 128, 288, and 512 SDS molecules were included. Each system contained 8, 32, 72, 128, 288, and 512 ion pairs (Na^+ and Cl^-) in a water phase composed of 24000 water molecules. The non-polar phase was composed of 2400 dodecane molecules. The equilibrated slab of water and ion molecules was first prepared. The desired number of surfactant molecules was added both on the top and bottom of the slab, in a 2D ordered lattice. A slab of pre-equilibrated dodecane molecules was then placed on top of the 2D slab with sufficient distance to avoid overlaps between molecules. Initial simulations at 100 bar of pressure were performed to connect the various phases. The system equilibration procedure was completed by relaxing the overall system at normal conditions for 50 ns.

The MD simulations of the overall system were performed with GROMACS 5.0.4 simulation package in a $NA_{xy}T$ ensemble [48,49], where A_{xy} is the area of the simulation box parallel of the water/-dodecane interface. The temperature was set to 300 K and was controlled with a velocity rescaling method [50] employing a coupling

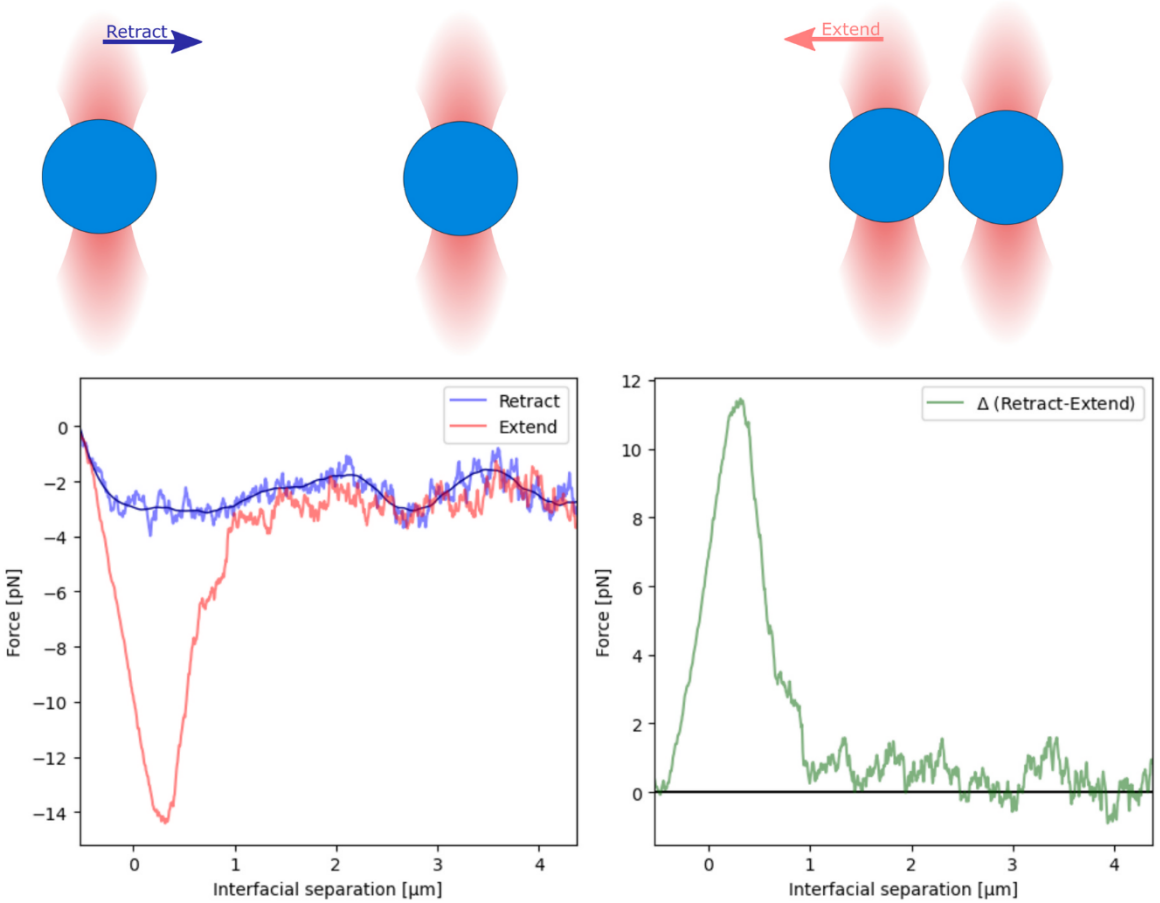

Fig. 1. *Top:* Illustration of trapped droplets retracted and extended and *Bottom left:* force versus distance plots for the two movements, colored accordingly, and *Bottom right:* the difference in force between retract and extend movements, giving the depletion force (the maximum point of the curve).

time of 0.1 ps. The pressure, P, was controlled by the Berendsen barostat and its normal component was maintained constant at 1 bar, with a time constant of 1.0 ps and compressibility coefficient of $4.5 \cdot 10^{-5}$ bar^{-1}. Electrostatic interactions were considered via Particle-Mesh Ewald summation, cut-off distances for nonbonded interactions were taken to be equal to 1.2 nm and the leapfrog algorithm solved the Newton equation of motion with 1 fs time steps interval. Periodic boundary conditions were applied along all spatial dimensions. The x and y directions of the simulation box for all the systems have a length of 16 nm. The height (z direction) depends upon the stage of the simulations.

For each system, the thin film was progressively reduced in a stepwise manner reflecting an artificial drainage procedure. At each step, a constant number of water molecules (400) were removed and the system re-equilibrated until the breakage of the thin film occurred. Each step followed a relaxation time of 10 ns and induced a thin film reduction of circa 0.4 Å. The procedure was iterated until the thin film was ruptured, and oil phases came into contact. The thin film thickness at the step preceding the film breakage event was used to estimate the critical thickness. When using this procedure the number of ions in the system remains constant, and the removal of water molecules, leading to reduced thin film thickness, will therefore lead to an increased local ion concentration. This approach is a judicious choice considering simulations limitations. In an experimental set-up, the ion concentration in the thin film is not known. It depends upon coalescence progression and on system properties beyond the reach of the molecular dynamics simulations (e.g. ion concentration in the bulk, total droplet surface area, surface surfactant concentration). Our simulation design aimed to provide a minimal disturbance to the system that undergoes a stochastic thin film breakage. The simulation captures the effect of the ion concentration on the thin film breakage by running multiple simulations at different ion concentrations.

3. Results and discussion

When using optical tweezers to study emulsions containing oil droplets of a wide size range, care must be taken when choosing droplet pairs for trapping so that their sizes do not change significantly between samples. The emulsion preparation procedure chosen has previously been shown to provide droplet populations with a suitable size range, and is a low-cost, time-efficient alternative to other techniques which did not prove to provide more narrow size-distribution [37]. While the methods used gave a wide spread of sizes in the droplet population, the droplet pairs used in the experiments were carefully selected based on microscopic imaging, ensuring a narrow spread of diameters for the droplets included in the OT-based investigations of coalescence.

3.1. Effect of ionic strength and surfactant density on depletion force

Immediately after emulsion homogenization, the liquid cell used in the OT experiments was filled with freshly prepared emulsion. An oil droplet was trapped in each of the two optical traps and the traps were calibrated using the procedures explained in previous sections. The two oil droplets were brought in contact by moving one optical trap until contact was obtained. This point was determined based on the obtained force-displacement curves, by inspecting each curve for signs of a collision force on the extension of traps. As shown in prior experiments [37], this point of contact might be challenging to identify, and overestimation of the displacement distance required might cause droplets to

coalesce. However, since the droplets used in the current study are stabilized by surfactants, the optimal contact points were, compared to our previous study [37], easier to achieve. The visual determination of size entails an inaccuracy due to the diffraction-limited resolution of light microscopy. The optical limit entails a 250 nm over or underestimation of the droplet diameter. However, these errors are not expected to significantly influence the calibration result for droplet pairs with diameters of ~ 9 μm.

The depletion force between droplet pairs was recorded as explained in the experimental section. Samples containing varying concentrations of ions and surfactant and droplet pairs in the size range 8–9 μm were inspected. The results revealed that the depletion force increases with increasing surfactant concentration (Fig. 2, top figure). This behavior was observed for all concentrations investigated.

The experimental series obtained by keeping the SDS concentrations constant and increasing the ionic strength confirmed this behavior in the sense that the depletion force increases with increasing SDS concentration for all ionic strengths (Fig. 2(*Bottom*). The sample containing 0.3μM SDS shows an unexpected low depletion force for the intermediate NaCl concentration of 20 mM. This is likely due to an underestimation of the depletion force due to insufficient contact of the droplets pairs during OT experiments. Furthermore, it is interesting to notice that the samples containing $\leq 30\mu$M SDS reach a maximum depletion force at the intermediate NaCl concentration investigated (20 mM). Whether this behavior is also followed by the 300 μM SDS series can not be determined based on the experimental data, due to the large error margin in the last data point in this experimental series. There may be several explanations for this effect. An increased density of the ionic surfactant on the interface might lead to a reduced charge difference between the interface and the bulk and thus reduced depletion force. Alternatively, the observations may be due to the increased pliability of the interface and thus the thin film, induced by the increasing surfactant density. This might lead to increased mobility of ions into the thin film, and thus effectively reduce the experienced depletion force. A third hypothesis to explain the findings involves the effect of the ionic surfactants on the mobility of ions when approaching the droplet interfaces to form a thin film. The presence of the surfactants reduces the mobility of the ions and therefore counteracts the establishment of a difference in concentration between bulk and thin film, and thus the osmotic pressure and depletion force. An elucidation of to what extent these explanations are valid, either alone or in combination, requires an improved understanding of the underlying mechanics on an atomistic scale, which we will return to in later sections of this paper.

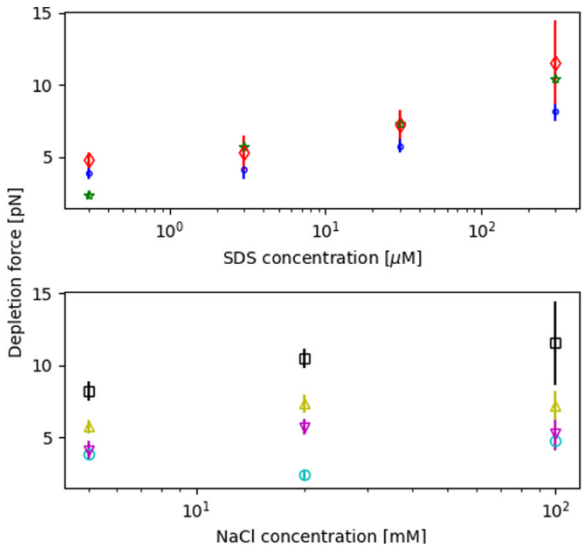

Fig. 2. Depletion force as a function of SDS concentration and NaCl concentration. *Top:* Depletion force as a function of SDS concentration. The NaCl concentration was kept constant at 5 mM (blue datapoints), 20 mM (red datapoints) and 100 mM (green datapoints). *Bottom:* Depletion force presented as a function of NaCl concentration. The SDS concentration was kept constant at 0.3μM (cyan), 3.0μM (purple), 30.0μM (yellow) or 300.0μM (black). Each data point represent the average of 20 measurements. The error bars in the plots represent the standard deviation for each data point, and all droplets investigated had a diameter in the range 8–9 μm.

3.2. Effect of ionic strength and surfactant density on droplet coalescence times

For the experimental conditions (SDS concentration and ionic strength) under which coalescence was observed, a second series of samples were prepared and investigated in order to determine the coalescence times. The coalescence times presented and discussed in the following represent average values calculated based on these observations.

In Fig. 3, the average coalescence time is reported as a function of increasing NaCl concentration for different SDS concentrations. At low salt and low surfactant concentration, the coalescence time exceeds the experimental limit of 6 min. This agrees with previous observations [37], where we noted that a certain bulk ionic concentration was necessary in order to observe coalescence within the time window investigated on OT. At the highest surfactant concentration investigated (300 mM), the coalescence time also exceeds the experimental limit, for most of the sample series. This illustrates that with the increasing density of surfactants a threshold will be reached where the interface is efficiently stabilized by the surfactants. However, the stability of the thin film appears compromised by a high concentration of salt at an intermediate concentration of surfactant (NaCl concentration in the range between 5 mM and 20.0 mM and SDS concentration in the range between 3.0 μM and 30.0 μM). We infer that this instability might be caused by a local perturbation driven by the surfactant molecules at the interface when present in sufficient density. The charged head-groups might promote a local over-concentration of ions that can facilitate the interaction between the two interfaces delimiting the thin film, promoting its breakage.

3.3. Properties and composition of the thin film prior to rupture

Thirty-six systems were studied to investigate the dependence of ion

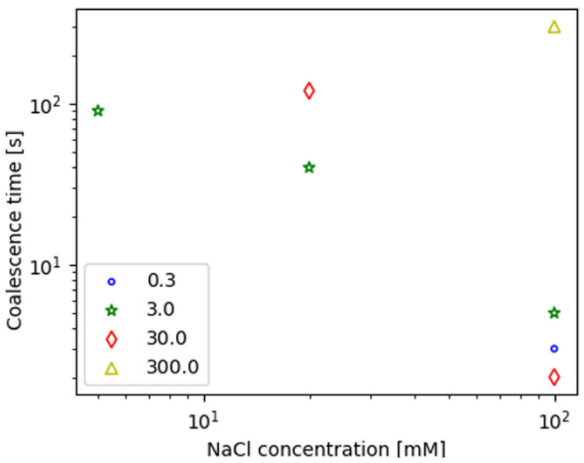

Fig. 3. Experimentally observed coalescence times under conditions of fixed SDS concentrations (colored series: blue=0.3μM, green=3.0μM, red=30.0μM, yellow=300.0μM) as a function of increasing concentration of NaCl. The data points shown in the figure are the average of 2–3 coalescence time measurements, and all oil droplets investigated had a diameter in the range 8–9 μm. A missing data point indicates that no coalescence was observed within the time period investigated (6 min).

and surfactant concentration on thin film breakage. The thickness of the aqueous thin film was for each system gradually reduced from an initial thickness that was sufficient to secure that the two oil-water interfaces did not interact with each other. The reduction in thickness was obtained by removing a fixed number of water molecules at each step. More precisely, 400 water molecules, resulting in a reduction in the film thickness equal to 0.4Å, were removed every 10 ns. If the water thin film were showing a uniform 2D density for the 10 ns step, a new step of water removal was performed. It should be stressed that the criterion for the stability assessment in simulations based on the 10 ns interval is considerably smaller than the one used in experiments based on the 6 min interval. Furthermore, simulations were aimed to estimate the critical thin film thickness, while optical tweezers measure the time elapsed from droplets contact to their coalescence. Thin film breakage is too immediate to be recorded separately (sub-microsecond scale).

Table 1 reports the composition and thickness of the thin film between the two oil droplets at the last simulation step prior to breakage and it is reported according to two different definitions: (i) *Top* thin film composed of water only, (ii) *Bottom* thin film composed by water, ions and surfactants (here defined as *critical thin film thickness*). To compute the thickness of the thin film reported in Table 1, the dimensions of the simulation box composed by different combinations of the system constituents has been computed, at the same conditions of pressure, temperature, and lateral box dimensions (16×16 nm) as in the main simulation set up. In the table, the overall simulation box thickness is obtained by accounting only for the contribution of the relevant constituents.

The surface surfactant densities were calculated by dividing the total number of molecules by the total interface area, 2 × [16 nm × 16 nm], and the reported ion concentrations were calculated prior to the first steps of the shrinking procedure, i.e. a 8.99×8.99×8.99 nm^3 water box.

From the Table 1, it can be asserted that the thin film rupture has a significant stochastic component, as noticeable deviations from linear trends have been reported. At the net of the statistical fluctuation, water presence in the thin film prior to breakage seems to not significantly be dependent upon surfactants nor ion concentration. The amount of water required to stabilize the thin film slightly increases for an increasing amount of surfactants.

For the critical thin film thickness, reported in Table 1(Bottom), more significant trends appear. The critical thin film thickness increases with increasing concentrations of surfactants and, to a lesser extent, of NaCl. To facilitate their visualization, the data reported in Table 1 (*Bottom*) is also presented as a 3D surface (Fig. 4).

When removing water molecules from the thin film, the local ion concentration increases. The ion mobility is reduced in the thin film due to the presence of charged surfactants and of the finite space. It should be reminded here that the local ion concentration depends also on bulk properties, but our relatively simplified simulation could not include these effects. Yet, it is worth reporting that the formation of small clusters of ions at the interface was observed for all systems with ionic concentrations larger or equal to 0.293 mol/L. This appears to be a heterogeneous nucleation promoted by the high local ion concentration promoted by the surfactants and by the finite space. In Fig. 5, the ion concentration profiles along the normal direction to the interface are plotted for different thin film thickness, for a simulation system of 0.293 mol/L NaCl and 14.976 mol/mm^2 SDS. It can be observed how the ions tend to accumulate in the water region, with an increasing concentration. In particular, Na^+ ions reach, from a bi-modal distribution to a Gaussian distribution for small thin films. Around the thin film critical value, the concentration of Na^+ and Cl^- ions become nearly identical, neutralizing the electrical double layer. This effect could, in

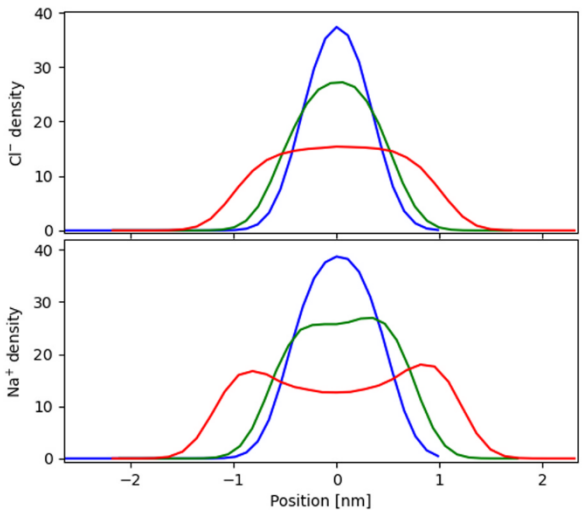

Fig. 4. Surface plot of data shown in Table 1(Bottom). The calculated critical thin film thickness is presented as a function of the concentration of NaCl in the solution as well as the interface density of surfactant on x- and y-axes respectively.

Table 1
Thin film thickness prior to breakage calculated for different NaCl concentration and surfactant surface concentration. *Top:* thickness of water layer only, and *Bottom:* thickness of thin film composed by water, ions, and surfactant (here defined as critical thin film thickness).

SDS mol/mm^2 NaCl mol/L	0.018	0.073	0.165	0.293	0.658	1.170
0.936	1.620	1.578	1.677	1.674	1.762	1.655
3.744	1.648	1.639	1.599	1.717	1.692	1.695
8.424	1.658	1.767	1.668	1.687	1.697	1.796
14.976	1.603	1.705	1.654	1.808	1.890	1.681
33.696	1.740	1.615	1.715	1.756	1.699	1.891
59.984	1.756	1.812	1.818	1.786	1.828	1.950
SDS mol/mm^2 NaCl mol/L	0.018	0.073	0.165	0.293	0.658	1.170
0.936	1.622	1.579	1.687	1.690	1.807	1.748
3.744	1.692	1.684	1.643	1.777	1.781	1.833
8.424	1.751	1.861	1.770	1.796	1.835	1.982
14.976	1.777	1.880	1.837	1.999	2.109	1.948
33.696	2.142	2.019	2.127	2.175	2.147	2.387
59.984	2.501	2.557	2.572	2.547	2.617	2.787

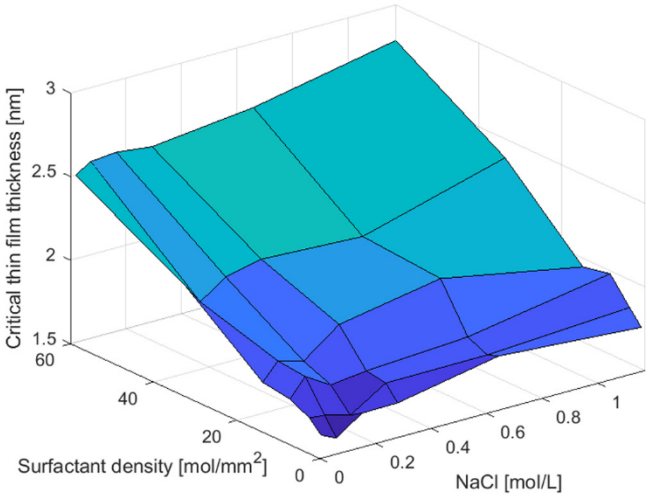

Fig. 5. Local concentration distribution of ions along the direction normal to the interface at different thin film thickness. *Top:* Cl^- ions and *Bottom:* Na^+ ions, ionic concentration 0.293 mol/L, SDS coverage 14.976 mol/mm^2. *Red line:* thin film thickness 3939 nm, *Green line:*, thin film thickness 3159 nm, *Blue line:* critical thickness of water film, 1.999 nm.

essence, contribute to lower the thin film stability and, hereby, promote coalescence. Furthermore, the increased ion concentration provides the necessary conditions to promote crystal seed formation. Ordered nano-cluster of ions were observed in different simulations, at sufficiently high local salt concentrations. These clusters can locally disrupt the interface properties. Surfactant molecules cannot freely rearrange, and the interfaces surrounding the thin film are, in effect, in contact via the salt grain, possibly inducing alterations in the overall thin film thickness. These observations are consistent with the reduction in the depletion force observed in Fig. 2 for the higher NaCl concentrations. Furthermore, the restricted mobility of the ions supports the hypothesis proposed above, stating that the presence of the surfactants reduces the

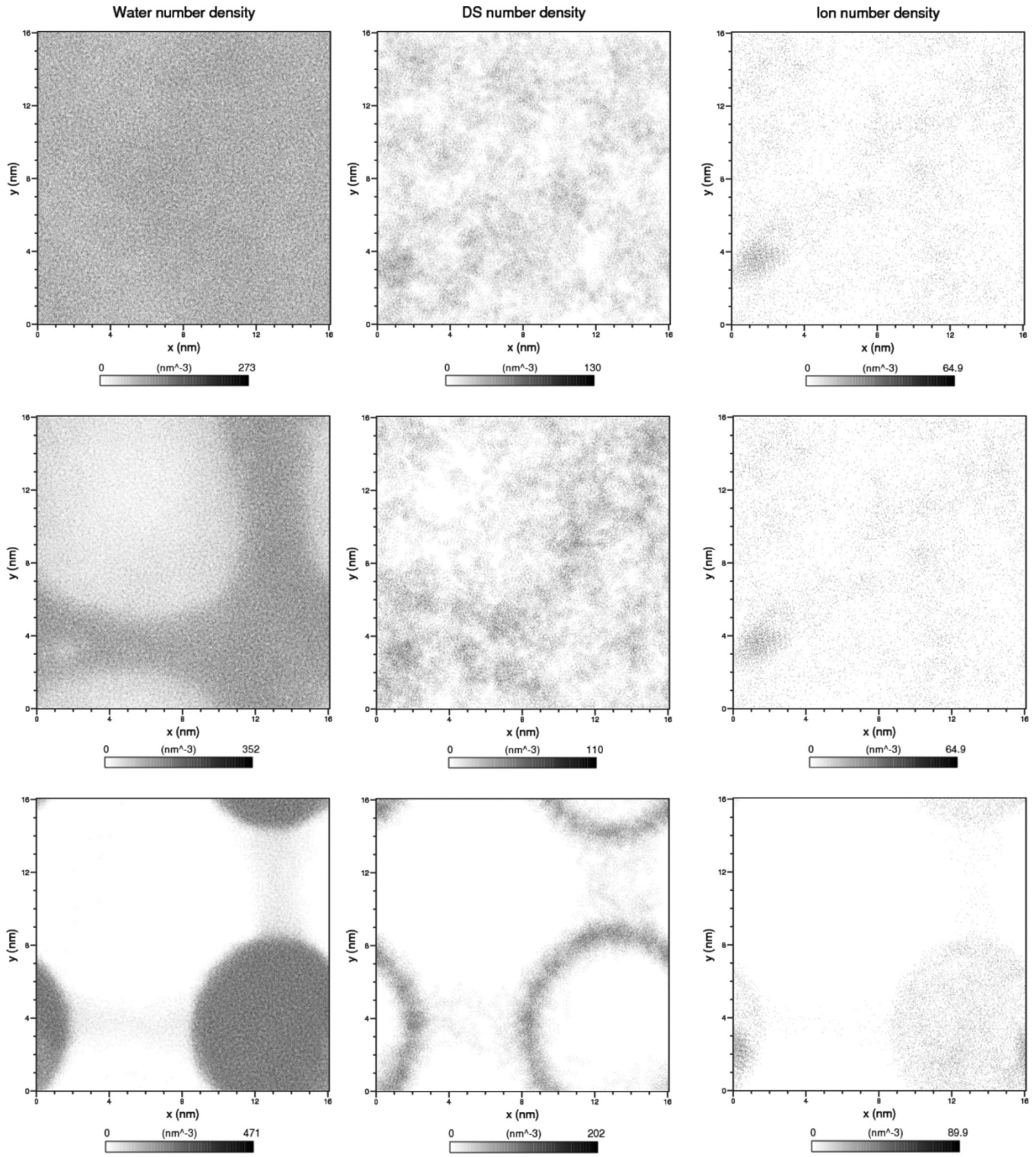

Fig. 6. Snapshots of MD simulation (Concentrations: SDS=14.976 mol/mm^2, NaCl=0.658 mol/L), showing the 2D density of ions (*left column*), water (*middle column*), and SDS (*right column*), for simulation trajectories during step-wise water molecule removal. *Top row:* # Water molecules (current film thickness) = 3200, oil phases are still separated. *Middle row:* # Water = 3100, system is beginning to show dimpling. *Bottom row:* # Water = 3000, the thin film is broken and the phases merge.

mobility of the ions and therefore counteracts the establishment of a charge difference between bulk and thin film, explaining the observed reduced depletion force.

To further elucidate the coalescence process, 2D density maps of water, surfactants, and ions have been generated for three different stages of step-wise water reduction and reported in Fig. 6 for the following case: density of SDS equal to 14.976 mol/mm^2, and concentration of NaCl equal to 0.658 mol/L. The plots were generated by averaging the *xy* position of the center of mass of each molecule/atom obtained from the trajectory produced in a shrinking step. The first row in Fig. 6 reports the 2D-densities at the critical thin film thickness, the second row reports the system conditions when the water layer is not any longer continuous (we consider the thin film to have been already ruptured, as the stability of this phase is extremely low) and the third row when the thin film is further compromised. The 2D density of water and surfactants is similar for all the studied cases in the system prior to the point where the critical thin film thickness is reached. The evolution of the thin film breakage can be, instead, different for different simulations of the same system. Depending on the initial phase of the breakage, the size and the shape of the water vacancy in the 2D density plot might vary. The stability of the second stage is also rather low, as most simulations evolve rather immediately to the third stage (third row) reported in Fig. 6. The water phase minimizes its surface area, generating a cylinder (for the periodic boundary condition assumption) or a sphere. For the case SDS= 14.976 mol/mm^2 and NaCl= 0.658 mol/L reported, ion nuclei can be observed already at the critical thin film stage. The nuclei seem to correlate with a region of water over-concentration in the second row of the 2D plot, probably contributing to the thin film breakage. In the third row, the ion nuclei are fully immersed in the water drop region.

It is worth reminding here that our simulation strategy is aimed to capture a structural description of the coalescence process. For instance, for simulation times longer than 10 ns, or different simulation setups, slightly different critical thin film thickness would result. A more accurate prediction of the film thickness prior to rupture could be obtained via rare event simulations where the probability of thin film breakage (and its rate), can be estimated for each thin film thickness. These approaches require a more involving set-up but they could directly account for the stochastic contribution in the process. The feature is also essential when studying the formation of nanocrystals that have been observed in the present simulations. While this phenomenon is of interest, the determination of the limiting conditions for its occurrence as well as the nucleation rate requires a dedicated investigation.

4. Conclusions

The effects of ionic strength and surfactant coverage on the depletion force acting between approached droplets were examined with optical tweezers and MD simulations. The stabilized emulsions investigated in the current study showed a similar response to depletion force by increasing ion concentrations as pristine emulsions [37]. This indicates that the presence of charges at the droplet interface did not impede the formation of a charge difference between thin film and bulk. The depletion force increased with increasing SDS concentration for all NaCl concentrations in the interval 5–100 mM. The samples containing $\leq 30\mu$M SDS reach a maximum in depletion force at the intermediate NaCl concentration investigated (20 mM), a behavior potentially also followed by the sample containing a higher concentration of SDS. This indicates that in the absence of a sufficient ionic strength required for the reduction of the double layer extent, the ionic surfactants provided a similar function to the liquid thin film. Furthermore, this effect appeared in our coalescence experiments, where samples of comparatively low NaCl concentration to previous work [37], still coalesced. Even with the higher interfacial coverage of stabilizing surfactants, the thin film was established and broke, for droplets approached to close proximity. The work here has thus improved upon the relatively brief exploration on approaching emulsion droplets with OT [27–30], and also with aid from theoretical simulations to explain the observed behavior in the liquid thin film.

The simulation data presented in the current paper indicate that the presence of the ionic surfactants reduces the mobility of the ions and therefore counteracts the establishment of a charge difference between bulk and thin film. This may be one factor explaining the observed decrease in the depletion force, although this would merit further investigation.

Both the experimental data and the simulations reveal that the coalescence process is strongly influenced by a stochastic behavior, leading to an inherent broad distribution of several variables, including the coalescence time. Still, the data reveal a reduced coalescence time with increased ionic strength of the surrounding solution, as expected based on previously published studies. The stabilizing effect of SDS on the droplet interface was sufficient to hinder coalescence when SDS was present at a concentration equal to or exceeding 300 μM, in combination with low ionic strength $\leq$ 20 mM.

Coalescence was not observed for the sample series containing the lowest SDS concentration investigated, but it was observed for SDS concentrations equal to 3 and 30 μM. A possible explanation was provided by the MD simulations. We estimated the thin film thickness prior to breakage (here defined as the critical film thickness), for a wide range of ions and surfactant concentrations. A dedicated approach to reproduce the mechanism of the coalescence process has been presented and adopted. The results presented reveal that the critical thin film thickness increases with increasing concentrations of surfactants and, to a lesser extent, NaCl. It appears that in the presence of surfactant, the water present in the thin film to stabilize the inter-phase slightly increases for increasing concentration of ions and surfactants. Furthermore, ions appear to increase the stability of the thin film. The electrical double layer is neutralized prior to the thin film breakage.

The increased local ion concentration and their reduced mobility in the thin film promoted the formation of small clusters of ions. The agglomerate presented, in some cases, an ordered structure, representing nanocrystals or crystal seeds. Their presence appears to influence thin film stability, promoting coalescence in samples of intermediate SDS concentrations (3 and 30 μM). While the formation of the ions agglomerate/nanocrystal is of certain interest, its simulation would require dedicated set-up and methodologies able to consider and quantify the stochastic contribution of the process.

Note that since the thin film rupture is also a stochastic process, different speeds of the artificial water removals will result in somewhat different estimates of the critical thin film thickness. More advanced simulation techniques [51–53,40,41], that we plan to report on in future publications, would allow the study of the thin breakage process without inducing any artificial bias, and analysis of the reactive paths [54–56] could be used to quantify whether the nanocrystal formation is in fact a trigger of the film breakage. This might provide a new mechanistic insight in the film breakage process that could possible be exploited to design operational techniques to reduce or accelerate coalescence. While the stability of emulsions depends on a large set of factors, the thin film breakage is one of the most significant bottlenecks in a coalescence process. An enhanced control and understanding of the mechanism can lead to better theoretical models and to the selection of more effective working conditions.

Author contributions

E. R., T.S.E. and M. S. were instrumental in the design and acquiring funding for the project. O. A., E. R. and M. S. designed the experiments. O. A. and M. S. developed optimized protocols for optical tweezer experiments. O. A. performed the experiments and did the experimental data analysis. E.R. designed, performed and analyzed the simulations. All authors were involved in the writing of the paper.

Declaration of Competing Interest

The authors declare that they have no known competing financial interests or personal relationships that could have appeared to influence the work reported in this paper.

Acknowledgements

This work was supported by the Research Council of Norway through their funding of the PETROMAKS 2 project number 267669.

References

[1] J.C. Slattery, L. Sagis, E.-S. Oh, Interfacial Transport Phenomena, Springer Science & Business Media,, 2007.
[2] I. Kralova, J. Sjöblom, G. Øye, S. Simon, B.A. Grimes, K. Paso, Heavy crude oils/particle stabilized emulsions, Adv. Colloid Interface Sci. 169 (2) (2011) 106–127.
[3] J.G. Speight, The Chemistry and Technology of Petroleum, CRC Press,, 2014.
[4] K. Kovalchuk, E. Riccardi, B.A. Grimes, Multiscale modeling of mass transfer and adsorption in liquid-liquid dispersions. 1. Molecular dynamics simulations and interfacial tension prediction for a mixed monolayer of mono-and tetracarboxylic acids, Ind. Eng. Chem. Res. 53 (29) (2014) 11691–11703.
[5] E. Riccardi, K. Kovalchuk, A.Y. Mehandzhiyski, B.A. Grimes, Structure and orientation of tetracarboxylic acids at oil-water interfaces, J. Dispers. Sci. Technol. 35 (7) (2014) 1018–1030.
[6] E. Riccardi, T. Tichelkamp, Calcium ion effects on the water/oil interface in the presence of anionic surfactants, Colloids Surf. A: Physicochem. Eng. Asp. 573 (2019) 246–254.
[7] B. Grimes, C. Dorao, S. Simon, E. NordgÅrd, J. Sjöblom, Analysis of dynamic surfactant mass transfer and its relationship to the transient stabilization of coalescing liquid-liquid dispersions, J. Colloid Interface Sci. 348 (2) (2010) 479–490.
[8] L. Leal, Flow induced coalescence of drops in a viscous fluid, Phys. Fluids 16 (6) (2004) 1833–1851.
[9] S.S. Jang, W.A. Goddard, Structures and properties of newton black films characterized using molecular dynamics simulations, J. Phys. Chem. B 110 (15) (2006) 7992–8001.
[10] Y. Mao, M. Cates, H. Lekkerkerker, Depletion force in colloidal systems, Phys. A: Stat. Mech. Appl. 222 (1–4) (1995) 10–24.
[11] A.I. Liapis, E. Riccardi, J.-C. Wang, Effects on the dynamic utilization of the adsorptive capacity of chromatographic columns induced by non-uniform ligand density distributions, J. Sep. Sci. 33 (17–18) (2010) 2749–2756.
[12] A. Ashkin, Acceleration and trapping of particles by radiation pressure, Phys. Rev. Lett. 24 (4) (1970) 156.
[13] A. Ashkin, J.M. Dziedzic, J.E. Bjorkholm, S. Chu, Observation of a single-beam gradient force optical trap for dielectric particles, Opt. Lett. 11 (5) (1986) 288–290.
[14] J.R. Moffitt, Y.R. Chemla, S.B. Smith, C. Bustamante, Recent advances in optical tweezers, Annu. Rev. Biochem. 77 (2008) 205–228.
[15] R. Huang, I. Chavez, K.M. Taute, B. Lukić, S. Jeney, M.G. Raizen, E.-L. Florin, Direct observation of the full transition from ballistic to diffusive brownian motion in a liquid, Nat. Phys. 7 (7) (2011) 576–580.
[16] Y. Deng, J. Bechhoefer, N.R. Forde, Brownian motion in a modulated optical trap, J. Opt. A: Pure Appl. Opt. 9 (8) (2007) S256.
[17] A. Pralle, M. Prummer, E.-L. Florin, E. Stelzer, J. Hörber, Three-dimensional high-resolution particle tracking for optical tweezers by forward scattered light, Microsc. Res. Tech. 44 (5) (1999) 378–386.
[18] L. Anderegg, L.W. Cheuk, Y. Bao, S. Burchesky, W. Ketterle, K.-K. Ni, J.M. Doyle, An optical tweezer array of ultracold molecules, Science 365 (6458) (2019) 1156–1158.
[19] R.M. Pettit, W. Ge, P. Kumar, D.R. Luntz-Martin, J.T. Schultz, L.P. Neukirch, M. Bhattacharya, A.N. Vamivakas, An optical tweezer phonon laser, Nat. Photonics 13 (6) (2019) 402–405.
[20] X. Wang, S. Chen, M. Kong, Z. Wang, K.D. Costa, R.A. Li, D. Sun, Enhanced cell sorting and manipulation with combined optical tweezer and microfluidic chip technologies, Lab Chip 11 (21) (2011) 3656–3662.
[21] N. Thammawongsa, F.D. Zainol, S. Mitatha, J. Ali, P.P. Yupapin, Nanorobot controlled by optical tweezer spin for microsurgical use, IEEE Trans. Nanotechnol. 12 (1) (2012) 29–34.
[22] S. Hadjialirezaei, G. Picco, R. Beatson, J. Burchell, B.T. Stokke, M. Sletmoen, Interactions between the breast cancer-associated muc1 mucins and c-type lectin characterized by optical tweezers, PLoS One 12 (4) (2017), e0175323.
[23] A.D. Ward, M.G. Berry, C.D. Mellor, C.D. Bain, Optical sculpture: controlled deformation of emulsion droplets with ultralow interfacial tensions using optical tweezers, Chem. Commun. (43) (2006) 4515–4517.
[24] A.L. Hargreaves, F. Gregson, A.K. Kirby, S. Engelskirchen, C.D. Bain, Microemulsion droplets in optical traps, J. Mol. Liq. 210 (2015) 9–19.
[25] D.A. Woods, C.D. Mellor, J.M. Taylor, C.D. Bain, A.D. Ward, Nanofluidic networks created and controlled by light, Soft Matter 7 (6) (2011) 2517–2520.
[26] W.-A.C. Bauer, J. Kotar, P. Cicuta, R.T. Woodward, J.V. Weaver, W.T. Huck, Microfluidic production of monodisperse functional o/w droplets and study of their reversible ph dependent aggregation behavior, Soft Matter 7 (9) (2011) 4214–4220.
[27] J. Nilsen-Nygaard, M. Sletmoen, K.I. Draget, Stability and interaction forces of oil-in-water emulsions as observed by optical tweezers-a proof-of-concept study, RSC Adv. 4 (94) (2014) 52220–52229.
[28] A. Chen, S.-W. Li, F.-N. Sang, H.-B. Zeng, J.-H. Xu, Interactions between micro-scale oil droplets in aqueous surfactant solution determined using optical tweezers, J. Colloid Interface Sci. 532 (2018) 128–135.
[29] A. Chen, S.-W. Li, D. Jing, J.-H. Xu, Interactions between colliding oil drops coated with non-ionic surfactant determined using optical tweezers, Chem. Eng. Sci. 193 (2019) 276–281.
[30] A. Chen, F. Wang, Y. Zhou, J.-h. Xu, In situmeasurements of interactions between switchable surface-active colloid particles using optical tweezers, Langmuir 36 (17) (2020) 4664–4670.
[31] M.R. Otazo, R. Ward, G. Gillies, R.S. Osborne, M. Golding, M.A. Williams, Aggregation and coalescence of partially crystalline emulsion drops investigated using optical tweezers, Soft Matter 15 (31) (2019) 6383–6391.
[32] M. Mitsunobu, S. Kobayashi, N. Takeyasu, T. Kaneta, Temperature-induced coalescence of droplets manipulated by optical trapping in an oil-in-water emulsion, Anal. Sci. 33 (6) (2017) 709–713.
[33] R. Power, J. Reid, S. Anand, D. McGloin, A. Almohamedi, N. Mistry, A. Hudson, Observation of the binary coalescence and equilibration of micrometer-sized droplets of aqueous aerosol in a single-beam gradient-force optical trap, J. Phys. Chem. A 116 (35) (2012) 8873–8884.
[34] B.R. Bzdek, L. Collard, J.E. Sprittles, A.J. Hudson, J.P. Reid, Dynamic measurements and simulations of airborne picolitre-droplet coalescence in holographic optical tweezers, J. Chem. Phys. 145 (5) (2016), 054502.
[35] A.E. Haddrell, R.E. Miles, B.R. Bzdek, J.P. Reid, R.J. Hopkins, J.S. Walker, Coalescence sampling and analysis of aerosols using aerosol optical tweezers, Anal. Chem. 89 (4) (2017) 2345–2352.
[36] S. Liu, Y. Hu, J. Xia, S. Fang, M. Duan, In situ measurement of depletion caused by sdbs micelles on the surface of silica particles using optical tweezers, Langmuir 35 (42) (2019) 13536–13542.
[37] O. Aarøen, E. Riccardi, M. Sletmoen, Exploring the effects of approach velocity on depletion force and coalescence in oil-in-water emulsions, RSC Adv. 11 (15) (2021) 8730–8740.
[38] T.S. Van Erp, P.G. Bolhuis, Elaborating transition interface sampling methods, J. Comput. Phys. 205 (1) (2005) 157–181.
[39] T.S. Van Erp, Dynamical rare event simulation techniques for equilibrium and nonequilibrium systems, Adv. Chem. Phys. 151 (2012) 27.
[40] A. Lervik, E. Riccardi, T.S. van Erp, Pyretis: a well-done, medium-sized python library for rare events, J. Comput. Chem. 38 (28) (2017) 2439–2451.
[41] E. Riccardi, A. Lervik, S. Roet, O. Aarøen, T.S. van Erp, Pyretis 2: an improbability drive for rare events, J. Comput. Chem. 41 (4) (2020) 370–377.
[42] M. Moqadam, A. Lervik, E. Riccardi, V. Venkatraman, B.K. Alsberg, and T.S. van Erp, Local initiation conditions for water autoionization, Proceedings of the National Academy of Sciences, 115, 20, E4569-E4576, 2018.
[43] E. Riccardi, E.C. Van Mastbergen, W.W. Navarre, J. Vreede, Predicting the mechanism and rate of h-ns binding to at-rich dna, PLoS Comput. Biol. 15 (3) (2019), e1006845.
[44] E. Riccardi, A. Krämer, T.S. van Erp, A. Ghysels, Permeation rates of oxygen through a lipid bilayer using replica exchange transition interface sampling, J. Phys. Chem. B 125 (1) (2020) 193–201.
[45] W.L. Jorgensen, D.S. Maxwell, J. Tirado-Rives, Development and testing of the opls all-atom force field on conformational energetics and properties of organic liquids, J. Am. Chem. Soc. 118 (45) (1996) 11225–11236.
[46] J.L. Abascal, C. Vega, A general purpose model for the condensed phases of water: Tip4p/2005, J. Chem. Phys. 123 (23) (2005), 234505.
[47] S. Abdel-Azeim, Revisiting opls-aa force field for the simulation of anionic surfactants in concentrated electrolyte solutions, J. Chem. Theory Comput. 16 (2) (2020) 1136–1145.
[48] D. Van Der Spoel, E. Lindahl, B. Hess, G. Groenhof, A.E. Mark, H.J. Berendsen, Gromacs: fast, flexible, and free, J. Comput. Chem. 26 (16) (2005) 1701–1718.
[49] M.J. Abraham, T. Murtola, R. Schulz, S. Páll, J.C. Smith, B. Hess, E. Lindahl, Gromacs: high performance molecular simulations through multi-level parallelism from laptops to supercomputers, SoftwareX 1 (2015) 19–25.
[50] G. Bussi, D. Donadio, M. Parrinello, Canonical sampling through velocity rescaling, J. Chem. Phys. 126 (1) (2007), 014101.
[51] T. van Erp, D. Moroni, P. Bolhuis, A novel path sampling method for the calculation of rate constants, J. Chem. Phys. 118 (2003) 7762.
[52] T. van Erp, Reaction rate calculation by tarallel path swapping, Phys. Rev. Lett. 98 (2007), 268301.
[53] E. Riccardi, O. Dahlen, T.S. van Erp, Fast decorrelating monte carlo moves for efficient path sampling, J. Phys. Chem. Lett. 8 (18) (2017) 4456–4460.
[54] T.S. van Erp, M. Moqadam, E. Riccardi, A. Lervik, Analyzing complex reaction mechanisms using path sampling, J. Chem. Theory Comput. 12 (11) (2016) 5398–5410.
[55] O. Aarøen, H. Kiær, E. Riccardi, Pyvisa: visualization and analysis of path sampling trajectories, J. Comput. Chem. 42 (6) (2020) 435–446.
[56] S. Roet, C.D. Daub, E. Riccardi, Chemistrees: Data-Driven Identification of Reaction Pathways *via* Machine Learning, J. Chem. Theory Comput 17 (10) (2021) 6193–6202.